As per UGC guidelines an electronic bar code is provided to secure your paper

International Journal for Modern Trends in Science and Technology
Volume 12, Issue 07, pages 123-138.
ISSN: 2455-3778 online
Available online at: http://www.ijmtst.com/vol12issue06.html
DOI: https://doi.org/10.5281/zenodo.20739614

Check for updates

Power Quality Enhancement and System Stability Improvement in Grid-Connected PV-Based EV Charging System Using Adaptive Controlled 9-Level MLI

Kavya Tambrallimath[1] | Dr. K. Siva Kumar[2]

[1]*PG Student, Dept. of Electrical & Electronics Engineering, Sri Venkatesa Perumal College of Engineering and Technology, Puttur, Andhra Pradesh, India*
[2]*Professor, Dept. of Electrical & Electronics Engineering, Sri Venkatesa Perumal College of Engineering and Technology, Puttur, Andhra Pradesh, India*

To Cite this Article
Kavya Tambrallimath & Dr. K. Siva Kumar (2026). Power Quality Enhancement and System Stability Improvement in Grid-Connected PV-Based EV Charging System Using Adaptive Controlled 9-Level MLI. International Journal for Modern Trends in Science and Technology, 12(07), 123-138. https://doi.org/10.5281/zenodo.20739614

Article Info
Received: 05 June 2026; Revised: 05 July 2026; Accepted: 08 July 2026.

KEYWORDS

Electric Vehicle (EV), Solar Photovoltaic, Nine-Level Multilevel Inverter, Adaptive Fuzzy Logic Controller, DC–DC Converter, Grid-to-Vehicle, Vehicle-to-Grid, Power Quality, System Stability, Total Harmonic Distortion

ABSTRACT

This paper presents a grid-connected photovoltaic (PV)-based electric vehicle (EV) charging system employing a Nine-Level Multilevel Inverter (9L-MLI) and an Adaptive Fuzzy Logic Controller (AFLC) to enhance power quality and system stability. The proposed system integrates a solar PV source with an EV battery through DC–DC boost and bidirectional buck–boost converters, enabling efficient energy management for Grid-to-Vehicle (G2V) and Vehicle-to-Grid (V2G) operations. The generated solar power is utilized for EV charging, local load support, and grid power injection depending on the operating conditions. A 9L-MLI is employed to produce a near-sinusoidal output voltage with reduced switching stress, lower total harmonic distortion (THD), and improved voltage quality compared with conventional multilevel inverter topologies. To achieve robust dynamic performance, an Adaptive Fuzzy Logic Controller is implemented for inverter switching control, DC-link voltage regulation, and grid current control under varying solar irradiance, load disturbances, and EV charging conditions. The adaptive fuzzy controller provides rapid disturbance rejection, accurate reference tracking, enhanced transient response, and improved steady-state performance compared with conventional PI-based control methods. The complete system is modeled and validated in MATLAB/Simulink. Simulation results demonstrate significant THD reduction, improved source current quality, stable DC-link voltage, enhanced power factor, efficient bidirectional power flow, and reliable operation under dynamic conditions. The proposed AFLC-based 9L-MLI

1. INTRODUCTION

The increasing demand for clean, reliable, and sustainable energy has accelerated the integration of renewable energy sources into modern electrical power systems [1]. Rapid industrialization, urbanization, and the continuous depletion of fossil fuel reserves have significantly increased global energy consumption while raising concerns regarding environmental pollution and greenhouse gas emissions [2]. Consequently, governments and researchers worldwide are promoting renewable energy technologies and electric vehicles (EVs) as effective solutions for reducing carbon emissions and achieving sustainable development goals [3]. Among various renewable energy resources, solar photovoltaic (PV) systems have emerged as one of the most attractive alternatives because of their clean energy generation, abundant availability, modular structure, and low maintenance requirements [4]. The declining cost of PV modules and continuous improvements in power electronic converters have further accelerated the deployment of PV systems in residential, commercial, and industrial applications [5]. Integrating PV generation with EV charging infrastructure provides an environmentally friendly and economically viable solution that minimizes dependence on conventional power plants while improving renewable energy utilization [6]. Electric vehicles have become an important component of future smart transportation systems because they eliminate tailpipe emissions and offer higher energy efficiency than conventional internal combustion engine vehicles [7]. The rapid penetration of EVs has resulted in a significant increase in charging demand, creating new challenges for utility distribution networks [8]. Large-scale EV charging can cause voltage fluctuations, transformer overloading, harmonic distortion, and poor power factor, and increased peak demand, thereby reducing overall power quality and system stability [9]. Therefore, efficient charging infrastructure integrated with renewable energy resources is essential for maintaining reliable grid operation while satisfying the growing demand for EV charging [10]. Grid-connected PV-based EV charging systems have attracted considerable attention because they simultaneously utilize renewable energy for battery charging while supporting the utility grid [11]. During periods of high solar irradiance, the generated PV power can directly charge EV batteries and supply local loads, whereas surplus energy can be injected into the utility grid [12]. Conversely, when solar power is insufficient, the required charging energy can be supplied from the utility grid to ensure uninterrupted operation [13]. Furthermore, bidirectional charging technology enables both Grid-to-Vehicle (G2V) and Vehicle-to-Grid (V2G) operating modes, allowing EV batteries to function as distributed energy storage systems capable of supporting grid operation during peak demand conditions [14]. The performance of grid-connected renewable energy systems is strongly dependent on the power electronic converter employed for energy conversion and grid synchronization [15]. Conventional two-level voltage source inverters are widely used because of their simple configuration; however, they produce output voltages with relatively high Total Harmonic Distortion (THD), increased switching losses, and higher voltage stress on semiconductor devices [16]. These limitations necessitate larger output filters, thereby increasing converter size, cost, and power losses [17]. To overcome these drawbacks, multilevel inverters (MLIs) have become one of the most promising converter technologies for medium- and high-power renewable energy applications [18]. By synthesizing multiple voltage levels, MLIs generate staircase voltage waveforms that closely approximate sinusoidal outputs, resulting in lower THD, reduced electromagnetic interference, improved converter efficiency, lower switching losses, and enhanced voltage quality [19]. Among the available multilevel inverter topologies, Neutral Point Clamped (NPC) [20], Flying Capacitor (FC) [21], and Cascaded H-Bridge (CHB) [22] converters have been widely investigated because of their excellent harmonic performance [23]. However, these conventional topologies generally require a large number of semiconductor switches, isolated DC sources, capacitors, and gate driver circuits, thereby increasing converter complexities, implementation cost, and control difficulty [24]. Recently, reduced-switch multilevel inverter topologies have gained significant research interest because they provide high-quality output voltage while minimizing the number of switching devices and associated power losses [25]. In particular, the Nine-Level Multilevel Inverter (9L-MLI) offers superior harmonic performance compared with conventional five-level and seven-level inverter topologies by generating a smoother staircase voltage waveform with lower switching stress and improved voltage quality [26]. These characteristics make the 9L-MLI highly suitable for renewable energy-based EV charging applications requiring efficient grid integration and improved power quality. In addition to inverter topology, the control strategy plays a vital role in determining the dynamic performance and stability of grid-connected PV-EV charging systems [27]. Conventional proportional-integral (PI) controllers are widely employed because of their simple design and implementation; however, their performance deteriorates under nonlinear operating conditions, renewable energy intermittency, parameter uncertainties, and sudden load variations [28]. Intelligent control techniques have therefore attracted considerable attention for improving converter performance, reference tracking, and DC-link voltage regulation. Among these techniques, the Adaptive Fuzzy Logic Controller (AFLC) has demonstrated excellent capability in handling nonlinear systems without requiring an accurate mathematical model [29]. By continuously adapting the control rules according to operating conditions, AFLC provides faster transient response, improved disturbance rejection, reduced steady-state error, accurate DC-link voltage regulation, and enhanced system stability under varying solar irradiance and EV charging conditions [30]. Motivated by these challenges, this paper proposes a grid-connected solar PV-based EV charging system employing an Adaptive Fuzzy Logic Controller (AFLC) and a Nine-Level Multilevel Inverter (9L-MLI). The proposed system integrates a solar PV array with a DC–DC boost converter, a bidirectional DC–DC buck–boost converter, and a reduced-switch 9L-MLI to facilitate efficient renewable energy utilization and bidirectional power transfer during both Grid-to-Vehicle (G2V) and Vehicle-to-Grid (V2G) operations [31]. The Adaptive Fuzzy Logic Controller regulates the DC-link voltage, controls inverter switching, and maintains synchronized grid current under varying irradiance and load conditions. The proposed converter produces a near-sinusoidal output voltage with reduced THD, improved power quality, enhanced power factor, lower switching losses, and superior dynamic performance compared with conventional control techniques. The complete system is modeled and validated using MATLAB/Simulink. Simulation results demonstrate significant improvement in DC-link voltage regulation, source current quality, inverter output performance, system stability, and overall converter efficiency, making the proposed approach suitable for next-generation renewable energy-integrated EV charging applications.

The main contributions of this work are summarized as follows:

1. Development of a grid-connected solar PV-based EV charging system using a reduced-switch Nine-Level Multilevel Inverter.
2. Design and implementation of an Adaptive Fuzzy Logic Controller for DC-link voltage regulation and inverter control.
3. Integration of DC–DC boost and bidirectional buck–boost converters to enable efficient G2V and V2G operation.

Significant improvement in power quality through reduced THD, improved power factor, and near-sinusoidal inverter output voltage.

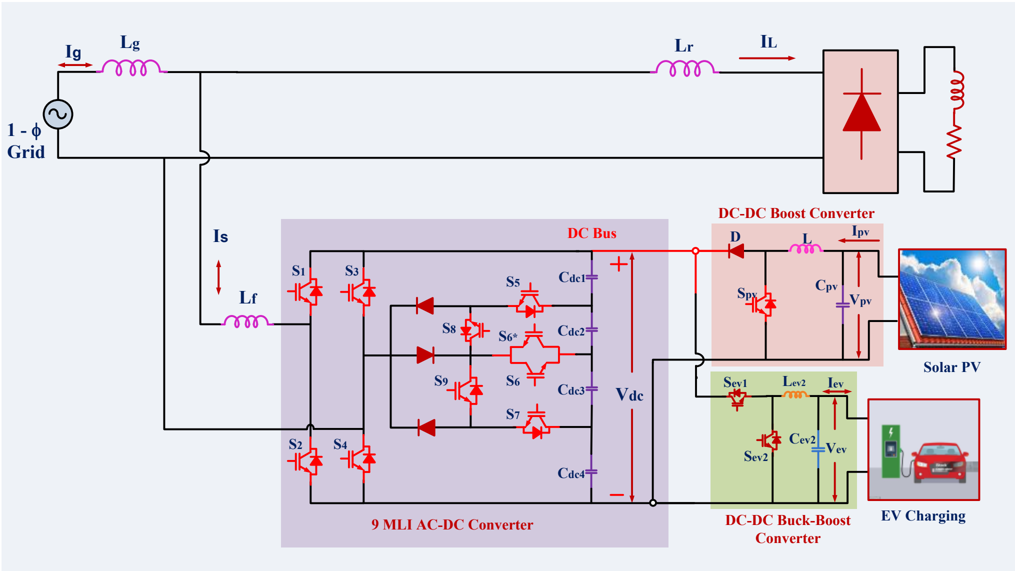

Fig. 1. Configuration of the Grid-Connected PV-Based EV Charging System Using a 9-Level Multilevel Inverter.

II. SYSTEM CONFIGURATION

Fig. 1 illustrates the proposed grid-connected photovoltaic (PV)-based electric vehicle (EV) charging system employing a Nine-Level Multilevel Inverter (9L-MLI) controlled by an Adaptive Fuzzy Logic Controller (AFLC). The system consists of a solar PV array, a DC–DC boost converter, a bidirectional DC–DC buck–boost converter, a DC-link capacitor, a reduced-switch 9L-MLI, an EV battery, and a single-phase utility grid. The PV array is connected to the common DC bus through the boost converter, which regulates the PV output voltage and ensures efficient power transfer to the DC-link. The EV battery is interfaced with the DC bus through a bidirectional DC–DC buck–boost converter, enabling both Grid-to-Vehicle (G2V) and Vehicle-to-Grid (V2G) operating modes. During G2V operation, the battery is charged using energy from the PV array and/or the utility grid, while in V2G mode, the stored battery energy is supplied back to the grid when required. The 9L-MLI converts the regulated DC-link voltage into a high-quality AC output with reduced harmonic distortion, improved voltage quality, and lower switching losses. The Adaptive Fuzzy Logic Controller regulates the DC-link voltage, controls the inverter switching signals, and maintains synchronized grid current under varying solar irradiance and load conditions. Consequently, the proposed system achieves enhanced power quality, improved system stability, efficient energy management, and reliable grid-connected operation.

III. SOLAR PV SYSTEM CONFIGURATION WITH INCREMENTAL CONDUCTANCE (INC) MPPT

The solar photovoltaic (PV) system serves as the primary renewable energy source in the proposed grid-connected EV charging system. As shown in Fig. 2, the PV array is connected to the common DC bus through a DC–DC boost converter controlled by the Incremental Conductance (INC) Maximum Power Point Tracking (MPPT) algorithm. The boost converter regulates the PV output voltage and ensures efficient extraction of the maximum available power under varying solar irradiance and temperature conditions. The regulated DC-link voltage is supplied to the Nine-Level Multilevel Inverter (9L-MLI) for grid integration and EV charging.

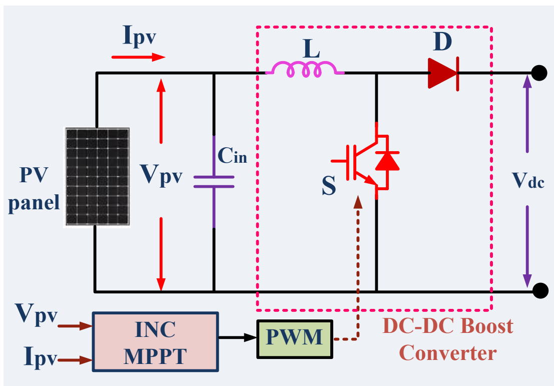

Fig. 2 solar PV INC MPPT DC-DC boost converter

The averaged transfer function of the boost converter relating the output voltage to the duty cycle is

$$\frac{V_{dc}(s)}{D(s)} = \frac{V_{in}}{(1-D^2)} \cdot \frac{1-\frac{sL}{R(1-D^2)}}{LCs^2+\frac{L}{R}s+1} \qquad (1)$$

Where L = Boost inductor, C = Output capacitor, R = Load resistance , Vin = PV input voltage

The inductor current transfer function is

$$\frac{I_L(s)}{V_{PV}(s)} = \frac{1}{Ls} \qquad (2)$$

The capacitor voltage transfer function is

$$\frac{V_{dc}(s)}{I_c(s)} = \frac{1}{Cs} \qquad (3)$$

The PV electrical power is

$$P_{PV} = V_{PV} \times I_{PV} \qquad (4)$$

and the generated energy is

$$E_{PV} = \int P_{PV}(t)\, dt \qquad (5)$$

The Adaptive Fuzzy Logic Controller receives the reference DC-link voltage and the measured voltage error to regulate the boost converter duty cycle. Consequently, the PV system continuously operates at its maximum power point while maintaining a stable DC-link voltage for the grid-connected inverter and EV charging system. The Incremental Conductance (INC) algorithm continuously monitors the PV voltage and current to determine the operating point of the PV array as shown in Fig.3 Based on the relationship between incremental conductance and instantaneous conductance, the controller adjusts the duty cycle of the boost converter to track the maximum power point (MPP). Compared with conventional Perturb and Observe (P&O) methods, the INC algorithm provides faster convergence, reduced steady-state oscillations, and higher tracking accuracy under rapidly changing environmental conditions.

The output power of the PV array is expressed as

$$P_{PV} = V_{PV} \times I_{PV} \qquad (6)$$

Where V_{PV} = PV array voltage (V), I_{PV} = PV array current (A)

At the maximum power point,

$$\frac{dP}{dV} = 0 \qquad (7)$$

Since

$$P = VI \qquad (8)$$

Then

$$\frac{d(VI)}{dV} = I + V\frac{dI}{dV} = 0 \qquad (9)$$

Therefore,

$$\frac{dI}{dV} = -\frac{I}{V} \qquad (10)$$

which represents the operating condition at the Maximum Power Point (MPP).

The operating regions of the INC algorithm are given by

$$\frac{dI}{dV} > -\frac{I}{V} \qquad (11)$$

(Operating point is on the left side of MPP)

$$\frac{dI}{dV} < -\frac{I}{V} \qquad (12)$$

(Operating point is on the right side of MPP)

$$\frac{dI}{dV} = -\frac{I}{V} \qquad (13)$$

(Maximum Power Point)

The INC controller generates the duty cycle for the boost converter according to

$$D(k) = D(k-1) + \Delta D \qquad (14)$$

Where D = Boost converter duty ratio, ΔD = Duty cycle increment

The boost converter output voltage is

$$V_{dc} = \frac{V_{PV}}{1-D} \qquad (15)$$

Where V_{dc} = DC-link voltage, D = Converter duty cycle

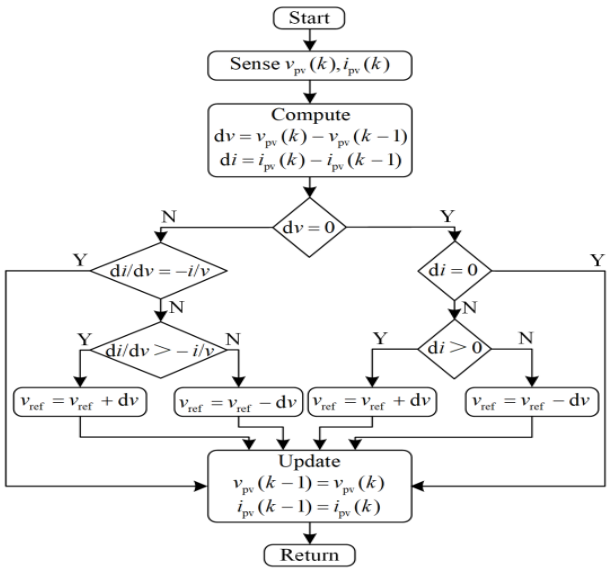

Fig. 3. Flow chat of modified incremental conductance maximum power point algorithm

IV. BIDIRECTIONAL DC–DC BUCK–BOOST CONVERTER FOR EV CHARGING SYSTEM

The proposed EV charging system employs a bidirectional DC–DC buck–boost converter to interface the electric vehicle (EV) battery with the common DC-link as shown in Fig.4. The converter enables efficient bidirectional power transfer, allowing both Grid-to-Vehicle (G2V) and Vehicle-to-Grid (V2G) operating modes. During G2V operation, the converter operates in buck mode to charge the EV battery by regulating the charging current and battery voltage. During V2G operation, the converter operates in boost mode, transferring the stored battery energy back to the DC-link and utility grid whenever additional power support is required. This bidirectional capability improves renewable energy utilization, enhances grid flexibility, and maintains stable DC-link voltage under varying operating conditions.

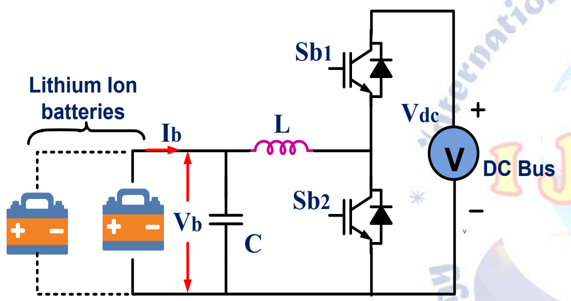

Fig.4 principle operation bidirectional dc-dc buck boost converter

A. Mathematical Model of DC–DC buck–boost converter

The dynamic characteristics of the bidirectional DC–DC buck–boost converter are analyzed using the Laplace-domain model. The converter consists of an inductor and a capacitor, which determine the transient response during battery charging and discharging. The mathematical model is obtained by applying Kirchhoff's Voltage Law (KVL) and Kirchhoff's Current Law (KCL) to the converter.

1) Inductor Current Transfer Function

The inductor voltage equation is expressed as

$$L\frac{di_L(t)}{dt} = V_L(t) \quad (16)$$

Applying the Laplace transform under zero initial conditions gives

$$\frac{I_L(s)}{V_L(s)} = \frac{1}{Ls} \quad (17)$$

This transfer function represents the dynamic relationship between the applied inductor voltage and the inductor current. It indicates that the inductor behaves as an energy storage element by limiting rapid current variations and reducing current ripple, thereby improving converter stability.

2) Capacitor Voltage Transfer Function

The capacitor current equation is

$$C\frac{dv_c(t)}{dt} = i_c(t) \quad (18)$$

The corresponding Laplace-domain transfer function is

$$\frac{V_c(s)}{I_c(s)} = \frac{1}{Cs} \quad (19)$$

The capacitor transfer function describes the voltage response with respect to the capacitor current. The DC-link capacitor stores electrical energy and suppresses voltage fluctuations caused by converter switching and load disturbances, thereby maintaining a stable DC-link voltage.

3) Buck Mode Transfer Function (G2V Operation)

During Grid-to-Vehicle (G2V) operation, the converter functions in buck mode to charge the EV battery. The small-signal transfer function relating the battery voltage to the converter duty cycle is

$$\frac{V_{bat}(s)}{D(s)} = \frac{V_{dc}}{LCs^2+\frac{L}{R}s+1} \quad (20)$$

Where $V_{bat}(s)$ = Battery voltage, V_{dc} = DC-link voltage. $D(s)$ = Duty cycle, L = Converter inductance, C = Output capacitance, R = Equivalent battery resistance

This second-order transfer function characterizes the converter dynamics during battery charging. The denominator determines the transient response, while the duty cycle controls the charging voltage applied to the EV battery.

4) Boost Mode Transfer Function (V2G Operation)

During Vehicle-to-Grid (V2G) operation, the converter operates in boost mode. The corresponding transfer function is

$$\frac{V_{dc}(s)}{D(s)} = \frac{V_{bat}}{(1-D)^2}\cdot\frac{1}{LCs^2+\frac{L}{R}s} + 1 \quad (21)$$

Where $V_{dc}(s)$ = DC-link voltage, V_{bat} = Battery voltage, D = Duty ratio

This transfer function shows the relationship between the converter duty cycle and the DC-link voltage during battery discharge. The converter boosts the battery voltage to the required DC-link level for supplying power to the utility grid.

5) Inductor Current Dynamic Transfer Function

The inductor current dynamics are represented by

$$\frac{I_L(s)}{V_{dc}(s)} = \frac{1}{Ls+R} \qquad (22)$$

This first-order transfer function describes the transient behavior of the inductor current. The inductor regulates the charging and discharging current, thereby reducing current ripple and improving converter efficiency.

6) Capacitor Voltage Dynamic Transfer Function

The DC-link capacitor dynamics are expressed as

$$\frac{V_{dc}(s)}{I_L(s)} = \frac{R}{RCs+1} \qquad (23)$$

This transfer function represents the relationship between the inductor current and the DC-link voltage. The capacitor acts as an energy buffer that maintains a nearly constant DC-link voltage during sudden load and power variations.

7) Battery Dynamic Model

The battery terminal voltage is expressed as

$$V_{bat} = V_{OC} - I_{bat}R_{int} \qquad (24)$$

Where V_{OC} = Open-circuit battery voltage, I_{bat} = Battery current, R_{int} = Internal battery resistance

The equation represents the electrical behavior of the battery by considering the voltage drop across its internal resistance. As the charging or discharging current increases, the terminal voltage changes accordingly.

8) Battery State of Charge (SOC)

The battery state of charge is calculated as

$$SOC(t) = SOC_0 - \frac{1}{Q_{bat}} \int_0^t I_{bat}(\tau)\, d\tau \qquad (25)$$

Where SOC_0 = Initial state of charge, Q_{bat} = Battery capacity (Ah)

The SOC equation estimates the remaining battery capacity by integrating the charging and discharging current over time. During G2V operation the SOC increases, whereas during V2G operation it decreases according to the exchanged energy.

B. EV Battery Current Controller

The EV battery current is regulated using a proportional–integral (PI) controller to ensure accurate charging and discharging current control. As shown in Fig.5, the reference battery current Ibat∗ is compared with the measured battery current Ibat, and the resulting error is processed by the PI controller. The controller output is used to generate Pulse Width Modulation (PWM) signals for the bidirectional DC–DC buck–boost converter, thereby maintaining the desired battery charging current during G2V operation and controlled battery discharging current during V2G operation.

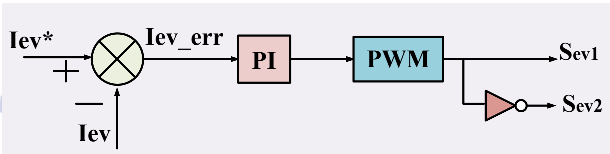

Fig. 5. Control Structure of the PI-Based Battery Current Controller

The battery current error is calculated as

$$e(t) = I_{bat}^{*}(t) - I_{bat}(t) \qquad (26)$$

Where $I_{bat}^{*}(t)$ = Reference battery current (A), $I_{bat}(t)$ = Measured battery current (A)

The PI controller output is expressed as

$$u(t) = k_P e(t) + k_i \int_0^t e(\tau)\, d\tau \qquad (27)$$

Where k_P = Proportional gain, k_i = Integral gain, $u(t)$ = PI controller output

The proportional term provides a fast response to changes in the battery current error, whereas the integral term eliminates the steady-state error and improves the current tracking accuracy.

The duty cycle generated by the controller is

$$D(t) = D_0 + u(t) \qquad (28)$$

Where D_0 = Initial duty cycle, $D(t)$ = Converter duty cycle

The PWM switching signal is generated by comparing the controller output with a high-frequency triangular carrier waveform and is expressed as

$$s = \begin{cases} 1, u(t) \geq V_{tr_i}(t) \\ 0, u(t) < V_{tri}(t) \end{cases} \qquad (29)$$

Where $V_{tr_i}(t)$ = Triangular carrier signal, S = PWM switching signal

The PI controller continuously updates the converter duty cycle based on the battery current error, ensuring accurate current regulation, reduced steady-state error, and smooth battery charging and discharging. The generated PWM pulses drive switches Sev1 and Sev2 in a complementary manner, enabling efficient operation of the bidirectional DC–DC buck–boost converter during both Grid-to-Vehicle (G2V) and Vehicle-to-Grid (V2G) modes. This control strategy improves charging performance, enhances converter stability, and maintains reliable operation of the proposed PV-based EV charging system.

V. NINE-LEVEL MULTILEVEL INVERTER (9L-MLI)

The proposed grid-connected PV-based EV charging system employs a Nine-Level Multilevel Inverter (9L-MLI) to convert the regulated DC-link voltage into a high-quality AC output voltage as shown in Fig.6 [31]. The inverter is operated using a Level-Shifted Sinusoidal Pulse Width Modulation (LS-SPWM) technique, in which a sinusoidal reference signal is compared with multiple level-shifted triangular carrier signals to generate the required switching pulses. The multilevel switching strategy enables the inverter to produce a staircase output voltage that closely approximates a sinusoidal waveform, thereby reducing harmonic distortion and improving output voltage quality.

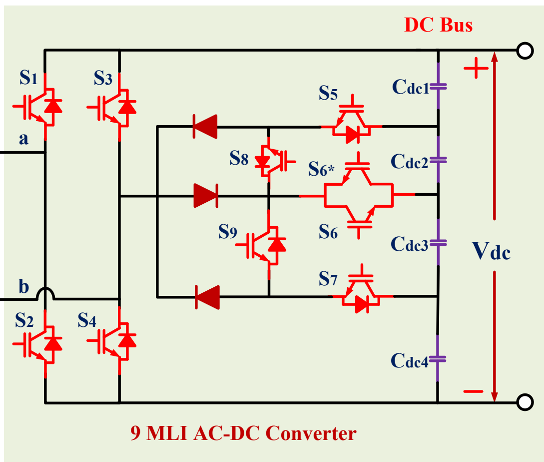

Fig. 6. Circuit Configuration of the Proposed Nine-Level AC–DC Converter.

The modulation index determines the amplitude of the inverter output voltage and is expressed as

$$M_a = \frac{A_m}{(N-1)A_C} \tag{30}$$

Where A_m and A_C represent the amplitudes of the reference and carrier signals, respectively, and NNN denotes the number of output voltage levels. Since the proposed inverter generates nine voltage levels, the modulation index becomes

$$M_a = \frac{A_m}{8A_C} \tag{31}$$

The frequency modulation ratio is defined as

$$M_f = \frac{f_C}{f_m} \tag{32}$$

Where f_C is the carrier frequency and fm is the fundamental frequency of the reference signal. A higher frequency modulation ratio improves the harmonic performance of the inverter by increasing the switching frequency while maintaining the desired output voltage.

The reference sinusoidal signal is represented as

$$V_{ref}(t) = A_m \sin(\omega t) \tag{33}$$

Where ω=2πfm. The carrier signal is generated using a triangular waveform and is expressed as

$$V_{car}(t) = A_c\, tr\, i(\omega_c t) \tag{34}$$

where ωc=2πfc. The reference and carrier signals are continuously compared to determine the switching states of the inverter.

The PWM switching function is defined as

$$S = \begin{cases} 1, V_{ref} \geq V_{car} \\ 0, V_{ref} < V_{car} \end{cases} \tag{35}$$

where S=1 represents the ON state of the corresponding switch, whereas S=0 denotes the OFF state. The generated switching pulses are applied to the inverter switches according to the selected switching sequence.

The output voltage of the proposed inverter is synthesized from nine discrete voltage levels and can be expressed as

$$V_0 = nV_{dc} \tag{36}$$

where V_{dc} is the DC-link voltage and

$$n = \left\{-1, -\frac{3}{4}, -\frac{1}{2}, -\frac{1}{4}, 0, \frac{1}{4}, \frac{1}{2}, \frac{3}{4}, 1\right\} \tag{37}$$

Accordingly, the output voltage levels are given by

$v_0 =$

$$\left\{-V_{dc}, \frac{-3}{4}V_{dc}, -\frac{1}{2}V_{dc}, -\frac{1}{4}V_{dc}, 0, \frac{1}{4}V_{dc}, \frac{1}{2}V_{dc}, \frac{3}{4}V_{dc}, V_{dc}\right. \quad (37)$$

These voltage levels are generated by properly controlling the switching states of the inverter, thereby producing a staircase waveform with significantly reduced harmonic content.

The instantaneous output voltage of the inverter is expressed as

$$v_0(t) = M_a V_{dc}\, sin(\omega t) \quad (38)$$

which indicates that the output voltage magnitude is directly controlled by the modulation index. Therefore, varying the modulation index allows regulation of the inverter output voltage without altering the DC-link voltage.

To avoid simultaneous conduction of complementary switches, the switching states satisfy the following condition:

$$s_i + \overline{s_i} = 1 \quad (39)$$

where Si and Si¯ denote the complementary upper and lower switching devices of the inverter leg.

The voltage increment between two adjacent output levels is given by

$$\Delta V = \frac{V_{dc}}{4} \quad (40)$$

Which ensures equal voltage spacing between consecutive output levels and contributes to smooth voltage transitions.

The number of output voltage levels generated by the inverter is determined as

$$N = 2m + 1 \quad (41)$$

where m is the number of positive voltage levels. For the proposed inverter,

$$N = 2(4) + 1 = 9 \quad (42)$$

Thus, the proposed 9-Level Multilevel Inverter effectively produces a near-sinusoidal output voltage with reduced switching stress and improved harmonic performance. The Level-Shifted Pulse Width Modulation (LS-SPWM) strategy enables accurate generation of the nine voltage levels while maintaining stable inverter operation, making the proposed topology highly suitable for grid-connected photovoltaic-based EV charging applications.

VI.ADAPTIVE FUZZY LOGIC CONTROLLER-BASED LEVEL- SHIFTED PWM CONTROL SCHEME

The proposed controller employs an Adaptive Fuzzy Logic Controller (AFLC) together with a TOSSI (Third-Order Sinusoidal Signal Integrator) algorithm and a Level-Shifted Pulse Width Modulation (LS-PWM) scheme to regulate the DC-link voltage and generate the switching pulses for the Nine-Level Multilevel Inverter (9L-MLI) as shown in Fig.7. The controller ensures accurate DC-link voltage regulation, effective current control, and synchronized power injection into the utility grid under varying solar irradiance and load conditions.

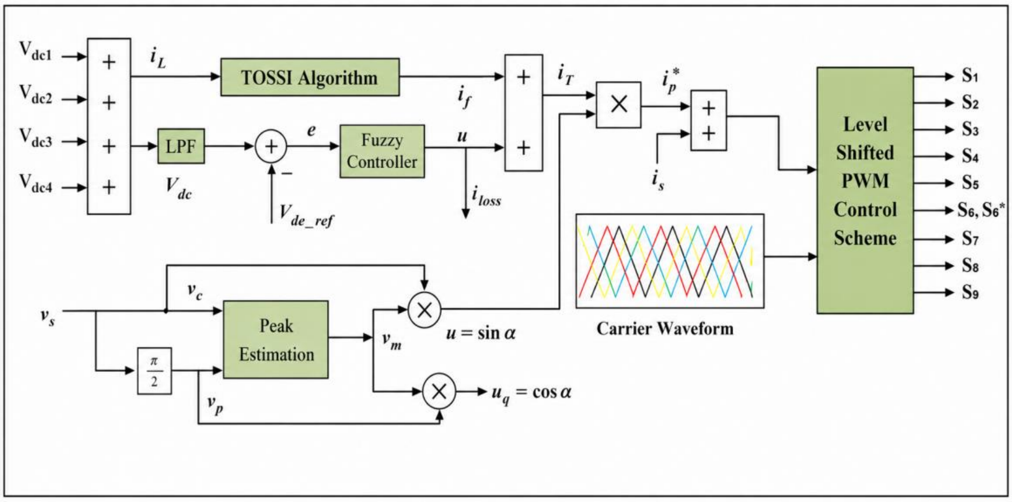

Fig. 7. Control Structure of the Proposed Fuzzy Logic Controlled Nine-Level Multilevel Inverter.

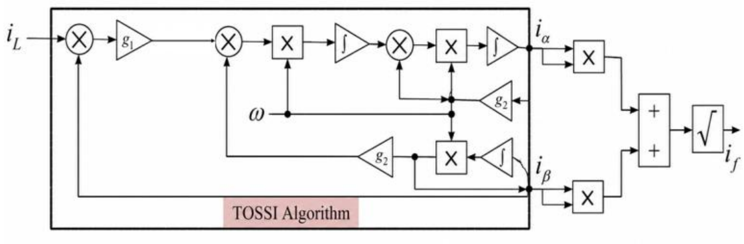

Fig. 8. Block Diagram of the TOSSI Algorithm for Fundamental Current Extraction.

Initially, the DC-link voltage is obtained by combining the capacitor voltages as

$$V_{DC} = V_{dC_1} + V_{dC_2} + V_{dC_3} + V_{dC_4} \quad (43)$$

Where V_{dc1}, V_{dc2}, V_{dc3}, and V_{dc4} are the individual capacitor voltages.

The measured DC-link voltage is filtered using a low-pass filter (LPF) to eliminate switching ripple and high-frequency noise. The voltage error is then calculated as

$$e(t) = V_{dc,ref} - V_{dC} \quad (44)$$

Where $V_{dc,ref}$ = Reference DC-link voltage, V_{dC} = Measured DC-link voltage

The change in voltage error is

$$\Delta e(t) = e(t) - e(t-1) \quad (45)$$

The Adaptive Fuzzy Logic Controller receives the voltage error and its variation as the input variables and generates the control signal

$$u(t) = F\big(e(t), \Delta e(t)\big) \quad (46)$$

where F(·) represents the fuzzy inference mechanism.

The output of the fuzzy controller is used to compensate the converter losses and is added to the fundamental current extracted by the TOSSI algorithm to obtain the reference current

$$i_T = i_f + i_{loss} \quad (47)$$

Where i_f = Fundamental current component, i_{loss} = Loss compensation current

The TOSSI algorithm extracts the fundamental component of the load current while rejecting harmonic components. The orthogonal current components are represented as

$$i_\alpha = i_f \sin(\omega t) \quad (48)$$

$$i_\beta = i_f \cos(\omega t) \quad (49)$$

Where ω=2πf, f = Grid frequency

The peak value of the grid voltage is estimated as

$$V_m = \sqrt{V_\alpha^2 + V_\beta^2} \quad (50)$$

The corresponding unit vectors are obtained as

$$u_\alpha = sin(\omega t) = \frac{V_\alpha}{V_m} \quad (51)$$

$$u_\beta = cos(\omega t) = \frac{V_\beta}{V_m} \quad (52)$$

The reference grid current is then generated by multiplying the unit vectors with the reference current

$$i_p^* = i_T u_\alpha \quad (53)$$

The actual grid current error is

$$i_s = i_p^* - i_g \quad (54)$$

Where

- ig = Measured grid current

The generated reference signal is compared with the level-shifted carrier signals to produce the PWM pulses according to

$$S = \begin{cases} 1, V_{ref} \geq V_{car} \\ 0, V_{ref} < V_{car} \end{cases} \quad (55)$$

Where

- V_{ref} = Reference modulating signal
- V_{car} = Level-shifted triangular carrier signal

Finally, the switching pulses generated by the LS-PWM controller are applied to switches S1–S9 of the proposed Nine-Level Multilevel Inverter.

VII. ADAPTIVE FUZZY LOGIC CONTROLLER DESIGN

The proposed Adaptive Fuzzy Logic Controller (AFLC) is employed to regulate the DC-link voltage and generate the control signal for the Level-Shifted PWM controller. The controller consists of four stages: fuzzification, rule inference, aggregation, and defuzzification as shown in Fig.9. The input variables are the DC-link voltage error and the change in voltage error, while the output variable is the control signal applied to the inverter.

The voltage error is calculated as

$$e(k) = V_{dc}^{*} - V_{dc} \quad (56)$$

where V_{dc}^{*} is the reference DC-link voltage and V_{dc} is the measured DC-link voltage.

The change in voltage error is

$$\Delta e(k) = \frac{de(k)}{dt} \quad (57)$$

A. Fuzzification

The input variables are converted into fuzzy variables using membership functions.

For a triangular membership function,

$$\mu(x) = \begin{cases} 0, x \leq a \\ \frac{x-a}{b-a}, a < x \leq b \\ \frac{c-x}{c-b}, b < x < c \\ 0, x \geq c \end{cases} \quad (58)$$

where

a,b,c are the triangular membership parameters.

B. Rule Evaluation

Each fuzzy rule is expressed as

$$R_i: IFe = A_i AND \Delta e = B_i THENu = C_i \quad (59)$$

The firing strength of the ith rule is

$$w_i = min[\mu_{A_i}(e), \mu_{B_i}(\Delta e)] \quad (60)$$

C. Aggregation

The fuzzy outputs from all activated rules are combined as

$$\mu_{out} = max(w_1, w_2, \ldots, w_n) \quad (61)$$

where n is the number of activated fuzzy rules.

D. Defuzzification

The crisp control signal is obtained using the centroid method

$$u = \frac{\int \mu_{Out}(x) x \, dx}{\int \mu_{Out}(x) \, dx} \quad (62)$$

For discrete implementation,

$$u = \frac{\sum_{j=1}^{n} w_i C_i}{\sum_{i=1}^{n} w_i} \quad (63)$$

where

- C_i is the output singleton.

E. Duty Cycle Update

The converter duty cycle is updated as

$$D(k) = D(k-1) + k_f u(k) \quad (64)$$

where

- k_f is the controller gain.

F. PWM Generation

The PWM pulse is generated by comparing the controller output with the carrier waveform

$$S = \begin{cases} 1, u > V_{tr\,i} \\ 0, u < V_{tri} \end{cases} \quad (65)$$

Adaptive Law

The adaptive gain can be updated as

$$k_f(k+1) = k_f(k) + \gamma e(k) \Delta e(k) \quad (66)$$

Where

- γ is the adaptation coefficient.

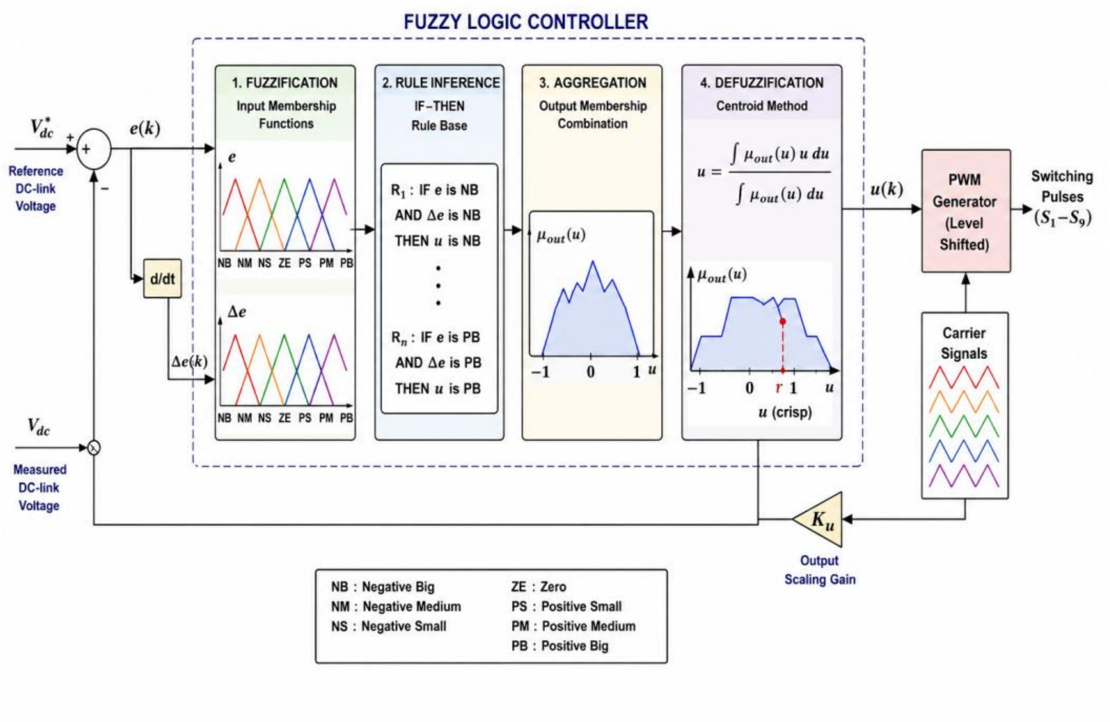

Fig. 9. Architecture of the Adaptive Fuzzy Logic Controller

VIII. SIMULATION RESULTS AND DISCUSSION

A. Grid Performance

Fig. 10 show the grid voltage (Vg), grid current (Ig), and nonlinear load current (IL) responses of the proposed Adaptive Fuzzy Logic Controller (AFLC)-based grid-connected PV-EV charging system. As shown in Fig. X(a), the grid voltage remains balanced and sinusoidal with a peak value of approximately ±230 V throughout the simulation period from 0 to 1.8 s, indicating proper synchronization between the proposed Nine-Level Multilevel Inverter (9L-MLI) and the utility grid. Fig. X(b) illustrates the grid current, which is maintained within approximately ±20 A during steady-state operation. During operating transitions at approximately 0.5 s, 0.8 s, 1.2 s, and 1.5 s, the current momentarily varies between −35 A and +35 A before quickly returning to its steady-state value, demonstrating the fast dynamic response and effective current regulation of the proposed controller. The nonlinear load current, which varies according to the connected nonlinear load demand and reaches a peak value of approximately ±11 A. The waveform exhibits the characteristic nonlinear behavior while the proposed controller effectively prevents these load current variations from affecting the grid current waveform. Consequently, the utility grid continues to supply a balanced sinusoidal current with improved power quality despite the presence of nonlinear load disturbances. These results verify the capability of the proposed AFLC-based control strategy to achieve stable grid synchronization, effective compensation of nonlinear load effects, and reliable grid-connected operation.

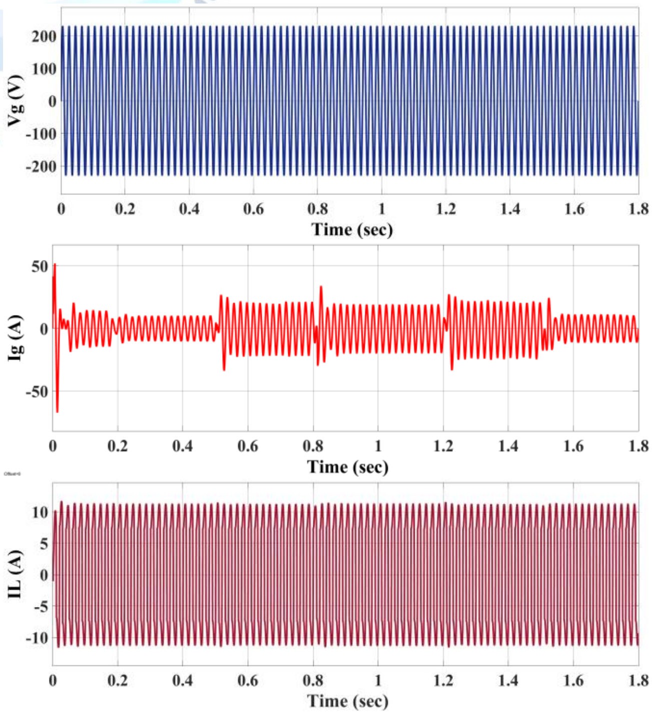

Fig. 10. Grid Performance Characteristics of the Proposed PV-Based EV Charging System

D. DC-Link Voltage Performance

Fig. 11 compares the DC-link voltage obtained using the conventional PI controller and the proposed Adaptive Fuzzy Logic Controller (AFLC). During system startup, both controllers regulate the DC-link voltage toward the reference value of 500 V. The PI controller exhibits an initial overshoot of approximately 560 V and noticeable oscillations before settling at the reference voltage. In contrast, the proposed AFLC achieves faster voltage regulation with a reduced overshoot of approximately 550 V and a shorter settling time. During transient operating conditions at around 0.5 s, 0.8 s, 1.2 s, and 1.5 s, the PI controller experiences comparatively larger voltage fluctuations, whereas the proposed AFLC rapidly suppresses the disturbances and restores the DC-link voltage to approximately 500 V with minimal oscillations. The steady-state voltage ripple is also significantly reduced using the proposed controller. These results demonstrate that the Adaptive Fuzzy Logic Controller provides superior DC-link voltage regulation, faster transient response, improved disturbance rejection, and enhanced overall stability of the proposed grid-connected PV-based EV charging system compared with the conventional PI controller.

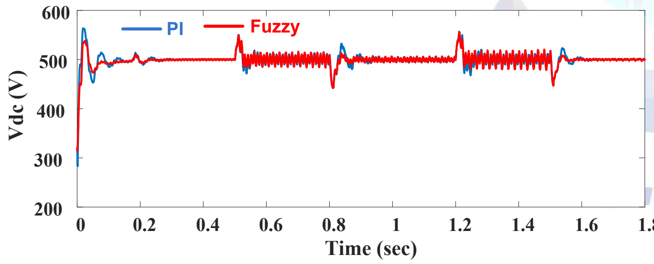

Fig. 11. DC-Link Voltage Regulation Using PI and Proposed Adaptive Fuzzy Logic Controllers.

B. Solar PV Performance

Fig. 12 present the solar photovoltaic voltage (VPV), current (IPV), and output power (PPV) characteristics. During startup, the PV voltage increases rapidly and reaches approximately 260 V at 0.12 s, after which it stabilizes around 225 V for the remainder of the simulation. The PV current initially remains at approximately 2.5 A, then increases to about 22 A during the high-power operating interval from 0.5 s to 1.5 s, before returning to approximately 2.5 A. Correspondingly, the PV output power increases from approximately 500 W during startup to nearly 5.1 kW under normal operating conditions and remains almost constant until 1.5 s, after which it decreases back to approximately 500 W. These results demonstrate effective maximum power extraction and stable PV operation under changing load conditions.

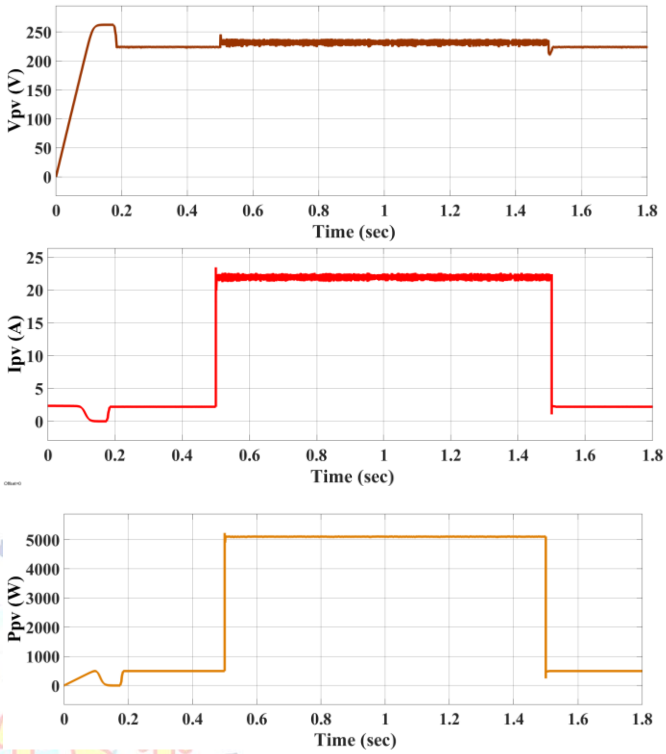

Fig. 12. Solar Photovoltaic Performance Characteristics of the Proposed EV Charging System.

C. Nine-Level Multilevel Inverter (9L-MLI) Performance

Fig. 13 illustrates the output voltage waveform of the proposed Nine-Level Multilevel Inverter (9L-MLI) controlled by the Adaptive Fuzzy Logic Controller. The inverter successfully generates nine distinct voltage levels of −500 V, −375 V, −250 V, −125 V, 0 V, +125 V, +250 V, +375 V, and +500 V, producing a staircase waveform that closely approximates a sinusoidal output. The output voltage reaches a peak value of approximately ±500 V and remains stable throughout the simulation period with smooth transitions between adjacent voltage levels. The Level-Shifted PWM (LS-PWM) switching strategy ensures accurate generation of the switching pulses, resulting in reduced switching stress and lower harmonic distortion. The generated multilevel voltage significantly improves the output waveform quality compared with conventional two-level and lower-level inverter topologies. These results demonstrate that the proposed 9L-MLI provides high-quality AC voltage with enhanced power quality, reduced voltage distortion, and stable operation for the grid-connected PV-based EV charging system.

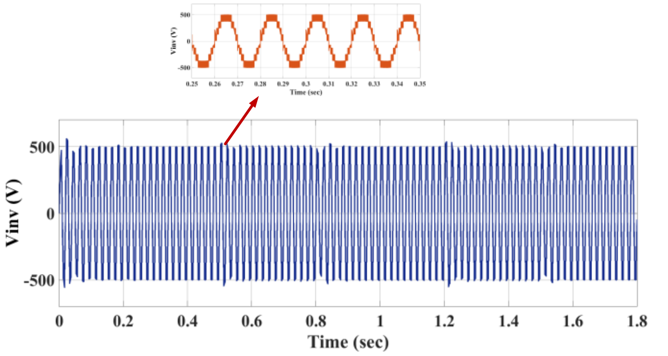

Fig. 13. Output Voltage Characteristics of the Proposed Nine-Level Multilevel Inverter (9L-MLI).

D. EV Battery Performance

Fig. 14 illustrate the DC-link voltage, inverter output voltage, EV battery voltage (VEV), battery current (IEV), and battery State of Charge (SOC). The proposed Adaptive Fuzzy Logic Controller regulates the DC-link voltage at the reference value of approximately 500 V, exhibiting lower overshoot and faster settling than the conventional PI controller during transient events. The nine-level inverter produces a staircase output voltage with a peak value of approximately ±500 V, confirming proper multilevel switching operation. The EV battery voltage remains nearly constant at approximately 216–217 V, indicating stable charging conditions. During charging, the battery current reaches approximately −24 A between 0.8 s and 1.2 s, while it remains close to 0 to −2 A outside the charging interval, demonstrating smooth transitions between charging states. Finally, the battery State of Charge (SOC) gradually increases from approximately 79.320% to 79.3212% during the charging period, confirming successful energy transfer from the photovoltaic system to the EV battery. Overall, the proposed Adaptive Fuzzy Logic Controller provides stable battery voltage regulation, accurate charging current control, and efficient battery energy management.

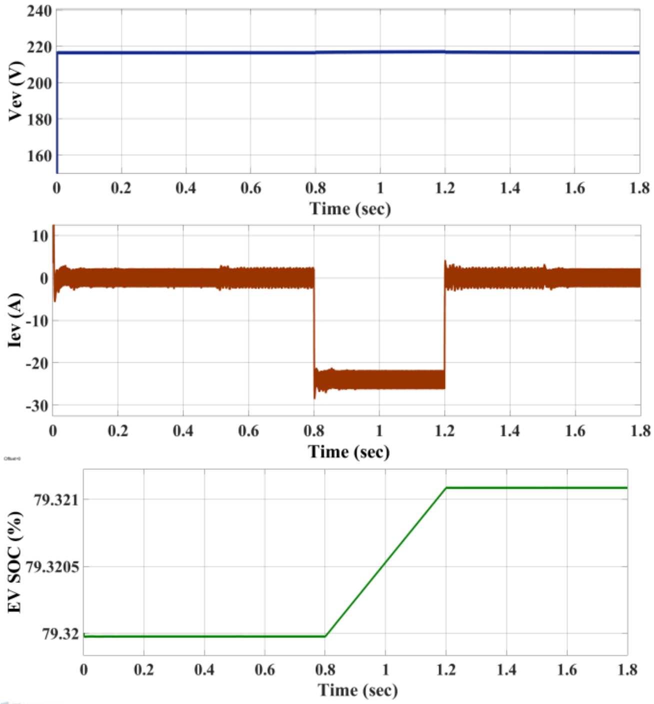

Fig. 14. EV Battery Charging Characteristics of the Proposed System

E. Grid Current Total Harmonic Distortion (THD)

Fig. 15 presents the Fast Fourier Transform (FFT) analysis of the grid current for the conventional 5-Level Multilevel Inverter (5L-MLI) and the proposed 9-Level Multilevel Inverter (9L-MLI). The proposed 9L-MLI achieves a Total Harmonic Distortion (THD) of 2.68%, whereas the conventional 5L-MLI exhibits a THD of 3.86%. The lower THD obtained with the proposed inverter demonstrates the effectiveness of the Adaptive Fuzzy Logic Controller and the Level-Shifted PWM switching strategy in reducing harmonic components in the grid current. The achieved THD of 2.68% is well below the 5% limit specified by IEEE Standard 519, confirming improved power quality and enhanced grid compatibility of the proposed PV-based EV charging system.

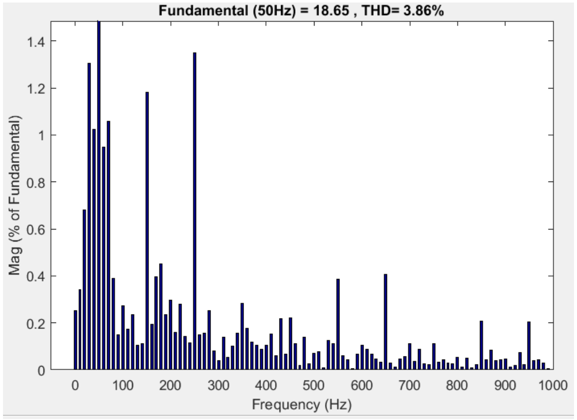

(a)

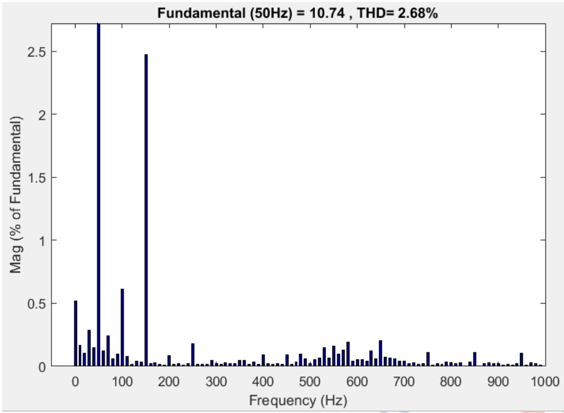

(b)

Fig. 15. FFT Analysis of Grid Current THD for the Conventional (a) 5-Level MLI and Proposed (b) 9-Level MLI

IX CONCLUSION

This paper presented an Adaptive Fuzzy Logic Controller (AFLC)-based grid-connected PV-powered EV charging system employing a Nine-Level Multilevel Inverter (9L-MLI) to enhance power quality and system stability. The proposed system effectively integrates the solar photovoltaic source, bidirectional DC–DC converter, EV battery, and utility grid to enable efficient Grid-to-Vehicle (G2V) and Vehicle-to-Grid (V2G) power transfer. The Adaptive Fuzzy Logic Controller provides superior DC-link voltage regulation with faster dynamic response, reduced overshoot, and improved disturbance rejection compared with the conventional PI controller. The proposed 9L-MLI generates a high-quality staircase output voltage with significantly reduced harmonic distortion, achieving a grid current THD of 2.68%, compared with 3.86% for the conventional 5L-MLI, thereby satisfying the IEEE 519 harmonic standard. Simulation results further demonstrate stable grid synchronization, effective nonlinear load compensation, efficient solar power extraction, and reliable EV battery charging with smooth voltage, current, and SOC characteristics. Overall, the proposed control strategy improves converter performance, power quality, system efficiency, and operational reliability, making it a promising solution for future renewable energy integrated smart EV charging applications.

Conflict of interest statement

Authors declare that they do not have any conflict of interest.

REFERENCES

[1]] Carrasco JM, Franquelo LG, Bialasiewicz JT, Galván E, PortilloGuisado RC, Prats MM, León JI, Moreno-Alfonso N. Power-electronic systems for the grid integration of renewable energy sources: A survey. IEEE Transactions on industrial electronics. 2006 Aug 7;53(4):1002-16.

[2] Singh B, Singh BN, Chandra A, Al-Haddad K, Pandey A, Kothari DP. A review of single-phase improved power quality AC-DC converters. IEEE Transactions on industrial electronics. 2003 Oct 31;50(5):962-81.

[3] Blaabjerg F, Teodorescu R, Liserre M, Timbus AV. Overview of control and grid synchronization for distributed power generation systems. IEEE Transactions on industrial electronics. 2006 Oct 2;53(5):1398-409.

[4] Rodriguez J, Lai JS, Peng FZ. Multilevel inverters: a survey of topologies, controls, and applications. IEEE Transactions on industrial electronics. 2002 Aug 31;49(4):724-38.

[5] Hossain E, Faruque HMR, Sunny MSH, Mohammad N, Nawar N (2020) A Comprehensive review on energy storage systems: types, comparison, current scenario, applications, barriers, and potential solutions, policies, and future prospects. Energies 13:3651. https://doi.org/10.3390/en13143651

[6] Lenka RK et al (2022) A unified control of grid-interactive off board EV battery charger with improved power quality. IEEE Trans Transp Electrif 9(1):920–933

[7] Heydari-doostabad H, O'Donnell T (2021) A wide-range highvoltage- gain bidirectional DC–DC converter for V2G and G2V hybrid EV charger. IEEE Trans Ind Electron 69(5):4718–4729

[8] Hannan MA, Hoque MM, Mohamed A, Ayob A. Review of energy storage systems for electric vehicle applications: Issues and challenges. Renewable and Sustainable Energy Reviews. 2017 Mar 1;69:771-89.

[9] Singh B, Jain V, Chandra A, Al-Haddad K (2021) Power quality improvement in a PV based EV charging station interfaced with three phase grid. In: Proceedings of the 47th annual conference of the IEEE industrial electronics society (IECON), pp 1–6

[10] Lenka RK et al (2022) PV integrated multifunctional off-board EV charger with improved grid power quality. IEEE Trans Ind Appl 58(5):5520–5532

[11] Chan CC. The state of the art of electric and hybrid vehicles. Proceedings of the IEEE. 2002 Feb 28;90(2):247-75.

[12] Yilmaz M, Krein PT. Review of battery charger topologies, charging power levels, and infrastructure for plug-in electric and hybrid vehicles. IEEE transactions on Power Electronics. 2012 Aug 23;28(5):2151-69.

[13] Khaligh A, Dusmez S. Comprehensive topological analysis of conductive and inductive charging solutions for plug-in electric vehicles. IEEE Transactions on Vehicular Technology. 2012 Aug 13;61(8):3475-89.

[14] Nayak S, Mohanty S (2023) Grid connected electric vehicle charging and discharging ratemanagementwith balance grid load. Electr Eng 105:575–592.

[15] Abu-Rub H, Malinowski M, Al-Haddad K. Power electronics for renewable energy systems, transportation and industrial applications. John Wiley & Sons; 2014 Jun 2.

[16] Zerka A, Ouassaid M, Maaroufi M. Strategic participation of electric vehicles in vehicle-to-grid within a microgrid system: A decentralized optimization approach. Results in Engineering. 2024 Dec 1;24:103144.

[17] Blaabjerg F, Teodorescu R, Liserre M, Timbus AV. Overview of control and grid synchronization for distributed power generation systems. IEEE Transactions on industrial electronics. 2006 Oct 2;53(5):1398-409.

[18] Peng FZ. A generalized multilevel inverter topology with self voltage balancing. IEEE Transactions on industry applications. 2001 Apr 30;37(2):611-8.

[19] S. Mamidala, A.K. Prajapati, R. Simhachalam, Modeling of buck converter charging station to improve the power quality using three phase single tuned harmonic filter for electric transportation, in: 2022 IEEE 2nd International Conference on Sustainable Energy and Future Electric Transportation (SeFeT), Hyderabad, India, 4-6 Aug. 2022.

[20] Rodriguez J, Bernet S, Steimer PK, Lizama IE. A survey on neutral-point-clamped inverters. IEEE transactions on Industrial Electronics. 2009 Sep 22;57(7):2219-30.

[21] Rodriguez J, Lai JS, Peng FZ. Multilevel inverters: a survey of topologies, controls, and applications. IEEE Transactions on industrial electronics. 2002 Aug 31;49(4):724-38.

[22] Malinowski M, Gopakumar K, Rodriguez J, Perez MA. A survey on cascaded multilevel inverters. IEEE Transactions on industrial electronics. 2009 Aug 28;57(7):2197-206.

[23] Peng FZ. A generalized multilevel inverter topology with self voltage balancing. IEEE Transactions on industry applications. 2001 Apr 30;37(2):611-8.

[24] Habib S, Kamran M, Rashid U. Impact analysis of vehicle-to-grid technology and charging strategies of electric vehicles on distribution networks–a review. Journal of Power Sources. 2015 Mar 1;277:205-14.

[25] Adupa C, Chidambaranathan VS. Design and performance evaluation of multilevel inverter for solar energy systems and electric vehicle charging with multi output active clamp forward converter. Science and Technology for Energy Transition. 2024;79:93.

[26] Uwagboe JO, Saha AK. A Comprehensive Review of Multilevel Inverter Topologies and Control Strategies for Grid-Connected Photovoltaic Battery Energy Storage Systems Integrating Active Power Filter. IEEE Access. 2025 Sep 26.

[27] Kouro S, Malinowski M, Gopakumar K, Pou J, Franquelo LG, Wu B, Rodriguez J, Pérez MA, Leon JI. Recent advances and industrial applications of multilevel converters. IEEE Transactions on industrial electronics. 2010 Jun 7;57(8):2553-80.

[28] Lemssaddak S, Hakam Y, Ait Elmahjoub A, Tabaa M, Zegrari M. Examining the current advancements in intelligent multilevel inverters for electric vehicle charging applications. Scientific African. 2025 Sep 1;29:e02799.

[29] Das SR, Mishra AK, Sahoo AK, Hota AP, Viriyasitavat W, Alghamdi NS, Dhiman G. Fuzzy controller designed-based multilevel inverter for power quality enhancement. IEEE Transactions on Consumer Electronics. 2024 Apr 16;70(2):4839-47.

[30] Miron A, Cziker AC, Beleiu HG. Fuzzy control systems for power quality improvement—A systematic review exploring their efficacy and efficiency. Applied Sciences. 2024 May 23;14(11):4468.

[31] Ali AI, Sayed MA, Mohamed EE, Azmy AM. Advanced single-phase nine-level converter for the integration of multiterminal DC supplies. IEEE Journal of Emerging and Selected Topics in Power Electronics. 2018 Sep 5; 7(3):1949-58.